frontiers | Frontiers in Energy Research

ORIGINAL RESEARCH
published: 18 July 2022
doi: 10.3389/fenrg.2022.936493

Metal-Organic Framework Supporting Fe_3O_4 Prepared by Microwave in Couple With NTP to Eliminate VOCs From Biofuel

Yan Gao[1,2], Qing Cao[1], Ning Guan[3], Zhanchao Zhang[2], Guolan Fan[2], Huawei Dou[1], Shijie Li[1], Qiang Wang[1] and Baoming Chen[1]*

[1]Shandong Province Carbon Neutrality Technology Innovation Center, School of Thermal Engineering, Shandong Jianzhu University, Jinan, China, [2]Shandong Province Jinan Ecological Environment Monitoring Center, Jinan, China, [3]School of Aeronautics, Shandong Jiaotong University, Jinan, China

In the production process of briquette biofuel, terpenes such as pinene and camphene, as well as non-terpenoid VOCs such as formic acid, acetaldehyde, and benzene, are generated during conditioning, drying and other procedures. Different catalysts of Fe_3O_4 supported by CoFe-ZIFs were prepared by thermal dissolution method and microwave dissolution method with changing the doping amount of iron. The structures of these catalysts were characterized by X-ray Diffraction (XRD), Fourier transform infrared spectrometer Fourier-Transformed InfraRed, thermogravimetric analysis (TG), and scanning electron microscope and the catalytic performance for α-pinene was tested on a fixed bed. The results show that, compared with the thermal dissolution method, the microwave dissolution method was easier to induce iron to form Fe_3O_4 grains with higher activity. At the same time, the grains did not affect the formation of CoFe-ZIFs structure. Fe_3O_4 supported on CoFe-ZIFs enhanced the catalytic activity and energy efficiency of the catalysts for α-pinene. Among the test samples, CoFe14-ZIF-W prepared by microwave method with Fe doping 14% mol exhibited the stable structural characteristics and the highest catalytic efficiency of 94.3% and energy efficiency of 8.11 g·kWh^{-1}, which provided a further possibility of practical application for the removal of VOCs from biomass.

Keywords: metal-organic framework, VOCs, microwave, non-thermal plasma, biofuel, magnetic

OPEN ACCESS

Edited by:
Jing Sun,
Shandong University, China

Reviewed by:
Shuai Tian,
Sun Yat-sen University, China
Jun Yan,
Shanghai Jiao Tong University, China

****Correspondence:***
Ning Guan
nn01006101@163.com

Specialty section:
This article was submitted to Process and Energy Systems Engineering, a section of the journal Frontiers in Energy Research

Received: *05 May 2022*
Accepted: *13 June 2022*
Published: *18 July 2022*

Citation:
Gao Y, Cao Q, Guan N, Zhang Z, Fan G, Dou H, Li S, Wang Q and Chen B (2022) Metal-Organic Framework Supporting Fe_3O_4 Prepared by Microwave in Couple With NTP to Eliminate VOCs From Biofuel. Front. Energy Res. 10:936493. doi: 10.3389/fenrg.2022.936493

1 INTRODUCTION

Biomass energy is the fourth largest energy source in the world besides the fossil fuels of oil, coal, and natural gas (Bhatia et al., 2020; Foong et al., 2020). It has become an important force in the international energy transformation, and plays an important role in coping with global climate change, energy supply and demand contradictions, and protecting the ecological environment (Gao et al., 2013; Manisalidis et al., 2020; Yoo et al., 2020; Li et al., 2021). During the manufacturing of biomass briquette fuel, the processes such as conditioning and drying lead to the evaporation of water and inevitably lead to the escape of volatile organic compounds (VOCs) inherent in the raw materials (Li X. et al., 2020; Zhu et al., 2020).

According to the different types of biomass raw materials and drying methods, there are many types of VOCs generated during processing, mainly including terpenes such as pinene and camphene, and non-terpenes such as formic acid, acetaldehyde, and benzene (Li H.-Y. et al., 2020; Li X. et al., 2020; Zhu et al., 2020). These VOCs have caused great harm to human health and ecological environment, and adversely affected the clean utilization of biomass briquette fuel (Manisalidis et al., 2020). In the drying process of pine and spruce, terpenes are the main components of VOCs released in wood drying. At the same time, the proportion of terpenes in the total extracts of spruce is 10–50%, while the proportion of that in pine wood is 25%–50% (Englund and Nussbaum, 2000). The turpentine smoke formed in the drying process of pine fuel contains a lot of terpenes, including α-pinene and β-pinene, which are very dangerous to the human body. The difference between α-pinene and β-pinene actually boils down to the difference in isomeric subtypes of "enantiomers" (Machado et al., 2019; Lee et al., 2020). The α-pinene and β-pinene are molecules made up of the same type and number of atoms (isomers) and shaped like mirror images of each other, and usually occur together in most plant and industrial compounds. Because of this, α-pinene and β-pinene have very similar effects on the human body, and relative differences in effects are difficult to distinguish (Pekgozlu and Ceylan, 2018; Bermudez et al., 2020). It is of great significance to study efficient and practical methods to remove the VOCs emitted during the manufacture and processing of biomass briquette fuel (Li H.-Y. et al., 2020).

The use of non-thermal plasma (NTP) technology to treat VOCs has the advantages of fast processing speed and simple operation (Guo et al., 2021b). However, the single use of NTP catalysis technology has disadvantages such as low CO_2 selectivity, low energy efficiency and the generation of by-products (George et al., 2021). These technical shortcomings greatly limit the popularization and application of this technology in the industrial field. In order to make up for the insufficiency of single NTP catalysis technology, catalysts synergistic NTP catalytic technology is carried out (Vandenbroucke et al., 2011). The synergistic effect of catalysts and NTP is mainly reflected in the fact that the catalyst can not only promote the transformation of energetic plasma, but also greatly reduce the production of toxic and harmful by-products (Cheng et al., 2019; Feng et al., 2020). Meanwhile, the presence of plasma can significantly improve the catalytic performance of the catalysts (Zhou et al., 2021). Therefore, the catalytic technology of catalysts synergistic NTP has gradually become a research focus in the treatment of VOCs (Huang et al., 2020; Liu et al., 2021). In the synergistic catalysis technology, the commonly used catalysts are mainly noble metals, transition metals, non-metal oxides, etc. The transition metals catalysts are the most widely studied and applied because of their abundant reserves and low cost of use (Gao et al., 2019a).

Metal-Organic Frameworks (MOFs) can be used as catalysts in NTP synergistic catalytic reactions due to their active chemical properties and controllable structure (Zhang et al., 2018; Vakili et al., 2020). MOFs are a new class of porous frameworks formed by the self-assembly reaction of metal ions and organic ligands (Guo Y. et al., 2021). Yaghi's group (Yaghi et al., 1995; Furukawa et al., 2013) reported the successful preparation of MOFs, which aroused great research interest from scholars all over the world, and made MOFs enter a stage of rapid development (Li H.-Y. et al., 2020). It has been extensively studied in recent years due to its tunable porosity and ease of fabrication. Nowadays, MOFs can be divided into different structures, such as IRMOF, MIL, ZIF, etc. ZIF materials are zeolite-like MOFs with topological structures synthesized by the reaction of Zn^{2+} or Co^{2+} with imidazole ligands, such as ZIF-2, ZIF-4, ZIF-8, ZIF-67, etc. (Wu et al., 2020; Shi et al., 2021) These ZIFs not only have the characteristics of MOFs, but also have the advantages of high stability of traditional zeolite materials (Qiu et al., 2021). Considering the influence of high-energy irradiation of NTP and the hot and humid environment formed by the catalytic oxidation of VOCs, the application of structurally stable ZIFs to synergistic NTP to catalyze VOCs can have better feasibility.

Over the past few years, many approaches have been explored to enhance the activity of ZIF-derived materials. The introduction of other active metal ions into ZIFs is considered to be a feasible strategy and has led to extensive research. With the deepening of research, more and more active metal ions have been introduced into ZIFs. Z.S. Li et al. (Li Z. S. et al., 2020) introduced Cu into ZIF-67 and the obtained structure of Co and Cu was uniformly arranged with higher dispersion and better catalytic effect. W.H. Zou et al. (Zou et al., 2021) prepared the new material by adding Mo into the structure of ZIF-67 to form abundant catalytic active centers and hollow structure, which exhibited excellent catalytic performance. The solvothermal synthesis method is simple in operation and easy to control the preparation conditions, and is the most commonly used method for the preparation of MOFs. However, the mechanical stirring process leads to a long time for material synthesis, and it is difficult to accurately control the crystal morphology (Gao et al., 2019b; Gao et al., 2019c). The preparation of MOFs by microwave is a relatively new method to synthesize nanomaterials in recent years (Jamshidifard et al., 2019; Ikreedeegh and Tahir, 2021). Due to the selective heating of objects by microwaves, the microwave preparation of MOFs has the advantages of high energy utilization, short reaction period and fast reaction speed (Safaei et al., 2019). In the solvothermal synthesis method, replacing the mechanical stirring process with the microwave dissolution process can significantly improve the dissolution efficiency of metal ions, shorten the preparation cycle, improve the preparation efficiency, and increase the yield.

In this study, ZIF structural materials were prepared by the microwave dissolution method or solvothermal synthesis method using cobalt and iron as two active elements. Under the NTP synergistic catalysis reaction of α-pinene, the catalytic efficiency and energy efficiency of CoFe-ZIFs with different proportions of cobalt and iron contents were investigated. The effect of microwave preparation method on the catalytic properties of bimetallic CoFe-ZIF was investigated. This study provides an experimental basis for the technological innovation of MOFs coupling with NTP to catalyze VOCs, and has important scientific value and practical significance for the clean utilization of biomass briquette fuel and the technological development of gas-phase multi-pollutant purification.

2 MATERIALS AND METHODS

2.1 Materials Preparations

All reagents were analytical grade without further purification. The reagents used mainly include $Co(NO_3)_2{\cdot}6H_2O$ (99.5%, Macklin, China), $Fe(NO_3)_3{\cdot}9H_2O$ (99.5%, Macklin, China), 2-methylimidazole (99.5%, Macklin, China), methanol (99%, Sinopharm, China), and deionized water. The preparation process is described below, taking the CoFe7-ZIF sample with Fe doping content of 7% as an example.

2.1.1 Preparation by Thermo Dissolution Method

The 541.26 mg $Co(NO_3)_2{\cdot}6H_2O$ and 56.56 mg $Fe(NO_3)_3{\cdot}9H_2O$ (the molar ratio of Fe was 7%) were dispersed into 30 ml methanol with heating and mechanically stirring at 75°C. The 4100 mg 2-methylimidazole was dispersed into 20 ml methanol, heated at 75°C with mechanical stirring. Then, the above two solutions were mixed and stirred for 15 min. After stirring, the mixture was kept at room temperature for 24 h. Next, the mixed solution was centrifuged at a centrifugal speed of 4000 r/min, and washed four times with methanol until the supernatant was transparent and colorless. The obtained purple-red precipitate was dried in a drying oven at 80°C for 12 h. Finally, the sample was ground and stored, and recorded as $CoFe_7$-ZIF. According to the above steps, the ratio of doping element was adjusted to prepare metal-organic framework materials with Fe molar ratio of 0%, 7%, 14%, 21% and 100%, recorded as $CoFe_0$-ZIF, $CoFe_7$-ZIF, $CoFe_{14}$-ZIF $CoFe_{21}$-ZIF, $CoFe_{100}$-ZIF, respectively.

2.1.2 Preparation by Microwave Dissolution Method

The preparation steps of the microwave dissolution method were basically the same as the preparation steps of the thermo dissolution method. The difference was that when the metal salt solution and the ligand solution are mixed and stirred, the microwave irradiation with a power of 900W for 20 min was used in Microwave Synthesis Reactor XHMC-1, combined with magnetic stirring at the surface magnetic field density 3200–3400 G and the magnetic attraction force 10.78N. The CoFe-ZIF samples prepared by microwave dissolution method were labeled as $CoFe_0$-ZIF-W, $CoFe_7$-ZIF-W, $CoFe_{14}$-ZIF-W, $CoFe_{21}$-ZIF-W, $CoFe_{100}$-ZIF-W according to the Fe molar ratio of 0%, 7%, 14%, 21% and 100%, respectively.

2.2 Materials Characterizations

Powder X-ray diffraction (XRD) patterns of CoFe-ZIFs were recorded on a Bruker D8 Advance powder diffractometer with monochromated Cu-Kα radiation source using a scan step size of 0.01°. The functional group compositions were tested via a BRUKER Tensor27 Fourier-Transformed InfraRed (FTIR) spectrometer. Thermogravimetric analysis (TG) was performed using Mettler-Toledo TGA/DSC 3 + synchronous thermal analyzer, with a temperature measurement range of 25–800°C and a heating rate of 20°C/min in a nitrogen atmosphere. The surface images of the samples were captured by a FEI Quanta 400 FEG scanning electron microscope.

2.3 ZIFs-NTP synergistic catalytic performance test

The experiment of CoFe-ZIFs cooperating with NTP to catalyze α-pinene was carried out in a fixed bed reactor, and the experimental system is shown in **Figure 1**. The experimental system consists of four parts: α-pinene generation device, plasma high-frequency power supply device, cooperative catalytic reaction device and gas analysis device. The evaporator controlled the α-pinene gas generation concentration. The initial α-pinene concentration was kept at 300 ppm. N_2 was used as the carrier gas. The concentration of VOCs was tested by HNRIKE PV6001 detector and the concentrations of CO, CO_2, N_2O, NO and NO_2 were tested by KZHI PTM600 composite gas analyzer. The total gas flow was stable at 2.25 L min^{-1}. Before each test, the concentration and flow of α-pinene at the inlet of the synergistic catalytic reaction device were kept stable for 5 min.

The main body of the synergistic catalytic reaction device was made of a cylindrical quartz tube with an inner diameter of 10 mm, a wall thickness of 1 mm and a length of 150 mm. The quartz tube acted as a blocking medium during discharge. A copper mesh with a length of 40 mm was wrapped around the center of the outer surface of the quartz tube as a ground electrode. A red copper rod with a diameter of 3 mm and a length of 300 mm was placed in the center of the quartz tube as a high-voltage electrode and fixed with sealant. There was an inlet/outlet port at each end of the reactor. Considering the possibility that the high-energy irradiation of NTP might cause the damage of ZIF structure, the catalyst particles were arranged at the downstream outlet of the copper mesh along the gas flow direction, which was closely connected with the NTP discharge area, but did not receive direct irradiation of the NTP discharge.

The size of catalyst particles affected the catalytic performance to a certain extent. The smaller the catalytic particles, the larger the specific volume surface area of the catalyst, and the more opportunities for VOCs to contact the active sites on the surface of the catalyst, resulting in the enhanced activity of the catalyst. However, catalyst particles that were too small resulted in large pressure losses during the gas flowing through the catalyst bed. Therefore, 500 mg of a sample with a particle size of 10–20 mesh was placed in the quartz tube reactor for each experiment, taking into account the dual effects of catalyst particle size on catalytic performance and pressure drop, based on published similar experiments and previous experimental experience of our group (Lu et al., 2019; Gao et al., 2021b). The plasma power supply adopted high voltage AC power supply. During the experiment, the input voltage was kept constant, and the input power of the plasma reactor was adjusted by changing the input current value. The discharge power of the reactor was taken as 10 W, 12 W, 14 W, 16 W and 18 W, respectively.

The evaluation of catalytic performance mainly considered α-pinene catalytic efficiency (η_{pinene}) and energy efficiency (η_{energy}), and the calculation formula was as follows (Gao et al., 2021a):

$$\eta_{pinene}\ (\%) = \frac{[pinene]_{in} - [pinene]_{out}}{[pinene]_{in}} \times 100\% \qquad (1)$$

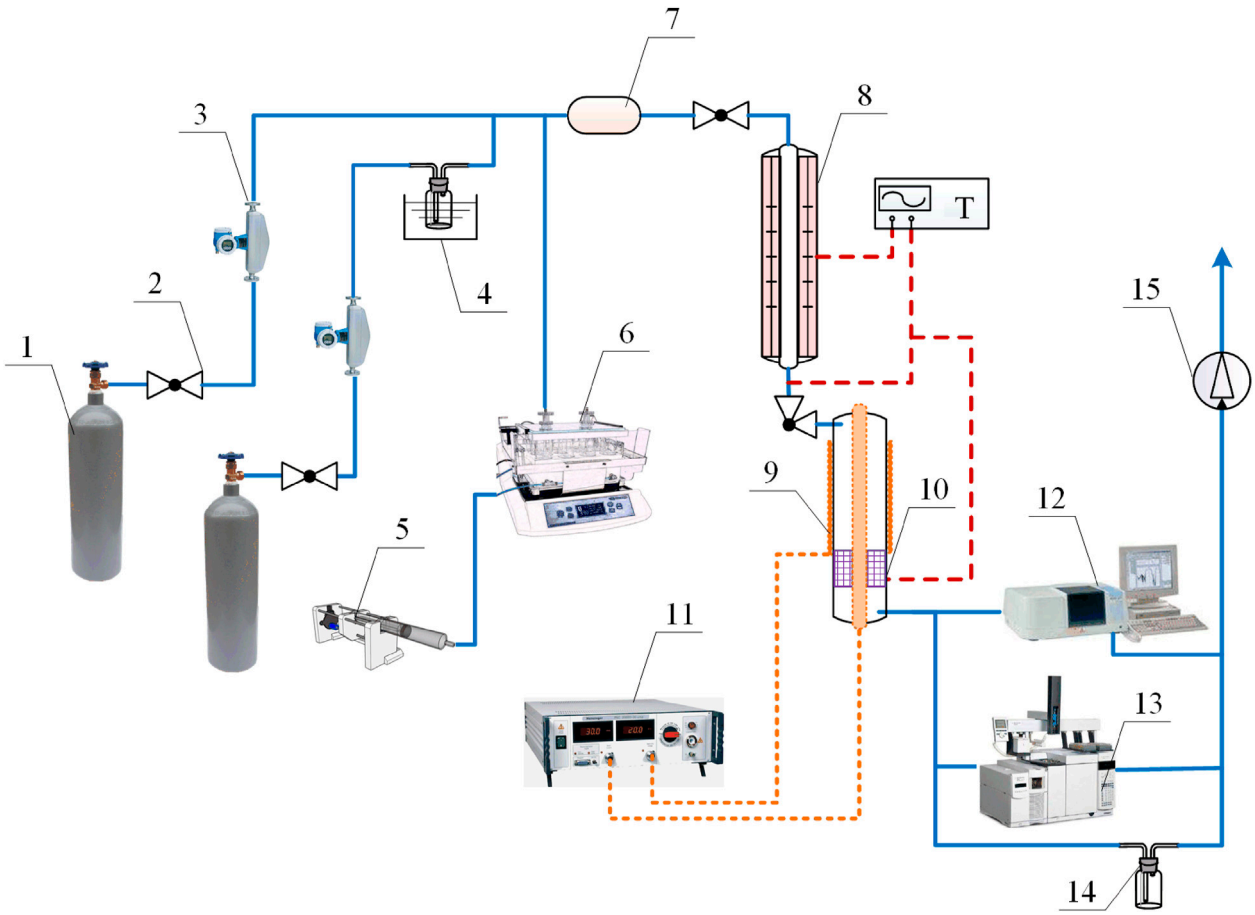

FIGURE 1 | ZIFs coupling NTP catalytic VOCs experimental device diagram: (1) Standard gas cylinder; (2) On-off valve; (3) Mass flow meter; (4) water evaporator; (5) VOCs injection pump; (6) VOCs evaporator; (7) Gas mixing cylinder; (8) Temperature control section; (9) NTP catalytic section (10) ZIFs catalysts (11) Plasma high-frequency power supply (12) VOCs analyzer (13) composite gas analyzer (14) Gas scrubber (15) induced draft fan.

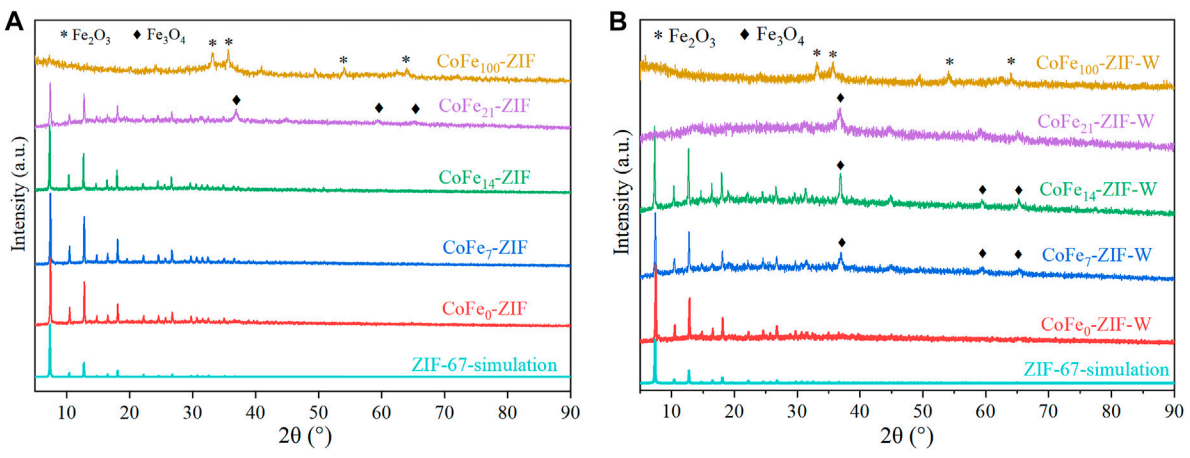

FIGURE 2 | XRD patterns of catalysts under different preparation conditions **(A)** thermo dissolution method **(B)** microwave dissolution method.

$$\eta_{energy}\ (g \cdot KWh^{-1}) = \frac{[pinene]_{in} \times \eta_{pinene} \times M \times 0.15}{SIE} \quad (2)$$

$$SIE\left(\frac{J}{L}\right) = \frac{P}{Q} \times 60 \quad (3)$$

Where, $[pinene]_{in}$ and $[pinene]_{out}$ were the α-pinene concentrations at the inlet and outlet of the plasma reactor, respectively. SIE was the input energy density; P was the input power; Q was the gas flow.

3 EXPERIMENTAL RESULTS AND DISCUSSION

3.1 Structural Characterization

3.1.1 XRD analysis

The XRD results of CoFe-ZIFs with different preparation methods and different Fe doping amounts were shown in **Figure 2**. It could be seen from **Figure 2A** that there were obvious X-diffraction characteristic peaks of 2θ at 7.36°, 10.43°, 12.78°, 14.75° and 18.11° in the four types of CoFe0-ZIF, CoFe7-ZIF, CoFe14-ZIF, and CoFe21-ZIF, which were entirely consistent with the simulated standard curve of ZIF-67 (Zhang et al., 2016; Zhou et al., 2017). These curves indicated that the prepared catalyst was successfully synthesized conforming ZIF-67 structure, and the CoFe-ZIFs had good crystallinity and complete crystal structure. However, the sample of CoFe100-ZIF (with Co molar content of 0) did not form a typical ZIF structure and only produced Fe_2O_3 crystals (PDF#33–0664) (Zheng et al., 2015). Meanwhile, the diffraction peaks of metal oxides were not strong enough. It could be due to the CoFe100-ZIF sample had not been calcined at high temperature for a long time, and the crystallization of the metal oxide was incomplete. In addition, it was not difficult to see that, with the continuous increase of Fe doping content from 0% to 100%, the crystallinity of ZIFs decreases continuously, at the same time, the diffraction angles of characteristic peaks also shifted at a certain extent. Taking the characteristic peak at 7.36° as an example, when Fe doping amount increases from 0% to 21%, 2θ shifted to the smaller angle by about 1.2°.

In the samples prepared by thermo dissolution method, as the Fe doping amount was 21%, more obvious X-ray characteristic diffraction peaks of Fe_3O_4 (PDF#26–1136) were found at the diffraction angles of 36.820°, 59.303° and 65.185°, corresponding to the crystal plane structures of (311) (511) and (440), respectively (Zhang et al., 2013; Zhang et al., 2015; Wu et al., 2020). This indicated that when the amount of Fe doping was small (≤14%mol), iron directly replaced Co and reacted with the ligand of 2-methylimidazole to form a bimetallic ZIF structure. While, as the Fe doping amount was too high (≥21%mol), the substitution ability of iron for cobalt was weakened and the excess iron atom began to precipitate in the form of Fe_3O_4 crystals. At the same time, the X-ray diffraction characteristic peaks of bimetallic FeCo-ZIFs were weakened at a certain extent, which demonstrated that the crystallinity of ZIFs was reduced. As only iron was used to react with the ligand of 2-methylimidazole without cobalt, no obvious ZIF structure was formed. In addition, the excess iron further transformed from Fe_3O_4 crystals to Fe_2O_3 crystals matching to the crystalline peaks at diffraction angles of 33.152° and 35.611°, corresponding to the crystal plane structures of (104) and (110) (Gao et al., 2018).

In the samples prepared by microwave dissolution method, the XRD curve of CoFe0-ZIF-W formed by Fe doping amount of 0 was almost the same as that of CoFe0-ZIF prepared by thermo dissolution method. For the CoFe7-ZIF-W sample with Fe doping content of 7%mol, there were obvious diffraction characteristic peaks of Fe_3O_4 crystal. The result showed that Fe_3O_4 crystals had begun to appear at the lower Fe doping amount under the combined action of microwave. It might be due to the irradiation of microwave made iron more easily to crystallize in the form of oxides. Compared with the samples of Fe doping content of 14%mol prepared by thermal dissolution method or microwave method, it could be seen that under the irradiation of microwave, although Fe_3O_4 crystals were formed, the structure of CoFe-ZIF was not affected and there was no visible change in the characteristic peaks or diffraction angles. Meanwhile, in the samples prepared by thermal dissolution method, it could be seen that when iron content reached to 14% mol, the characteristic peaks of Fe_3O_4 were more obvious, which proved the crystallinity of Fe_3O_4 increased. However, when the iron doping content raised above 21% mol, the ZIF structure did not appear in the catalyst, but mainly component existed in the form of Fe_3O_4. It could be attributed to the coordination bonds in ZIF were broken under the high-energy irradiation of microwaves, which accelerated the active Fe^{3+}/Fe^{2+} ions to produce metal oxide crystals combined with oxygen atoms (Wang et al., 2018; Chen et al., 2020), as a result, the ZIF structure suddenly disappeared.

In general, under microwave irradiation, Fe_3O_4 crystals were formed based on the excessively doped iron, while the crystal structure of ZIF formed by non-excess iron and ligand did not change significantly. Due to the redox characteristics of Fe^{3+}/Fe^{2+}, the thermal dissolution method could replace cobalt with iron at the greatest extent to form metal nodes and did not cause the redox of Fe^{3+} to form metal oxides, ensuring the stable crystallization of CoFe-ZIF. Microwave dissolution method endowed $Fe^{3+}$with more energy. The energized Fe^{3+} was easily transformed into other valence substances or combined with oxygen to produce oxide crystals. Therefore, a smaller amount of iron doping could be induced to form Fe_3O_4 crystals during the dissolution process of microwave, and at the same time, the stable crystallization of CoFe-ZIFs could still be guaranteed.

3.1.2 FTIR analysis

The prepared catalysts under different conditions were analyzed by FTIR spectroscopy, as shown in **Figure 3**. The interaction of the functional groups of various organic linkers in the samples could be obtained by analyzing the characteristic peaks of the infrared spectrum. Most of the absorption peaks in various catalysts were caused by the vibration of the ligand of 2-methylimidazole. The absorption peaks around 1400 cm^{-1} and 1300 cm^{-1} was assigned to stretched bands of different groups vibrations in the imidazole ring of 2-methylimidazole (organic linkers of ZIF) (Li et al., 2019). In addition, the absorption peak

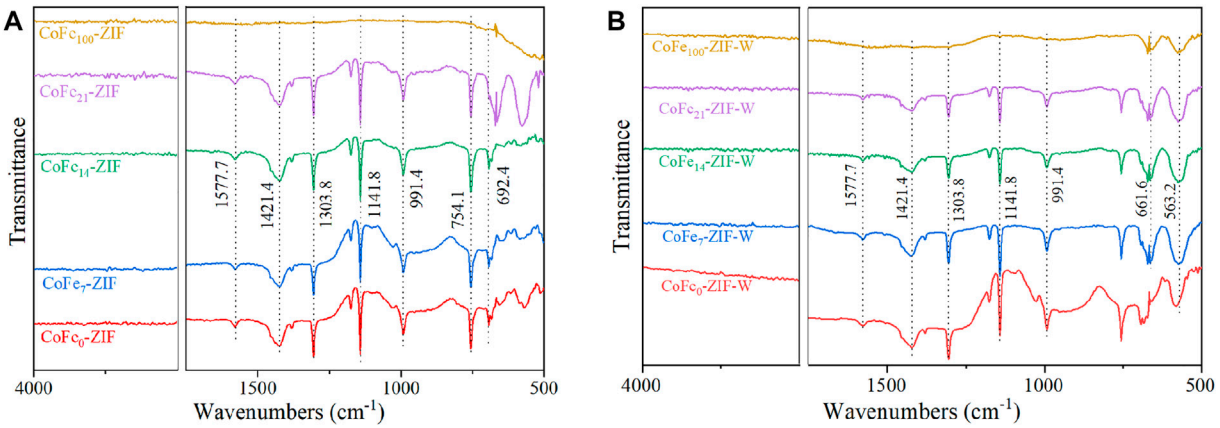

FIGURE 3 | FTIR spectra curves of catalysts under different preparation conditions **(A)** thermo dissolution method **(B)** microwave dissolution method.

near 1577 cm^{-1} was attributed to the stretching vibration of C=N in imidazole. The peaks near 1140 cm^{-1} and 1000 cm^{-1} were the stretching vibration peaks of the C-N and Co-N bonds (Hu et al., 2011). Except for the sample with Fe doping content of 100%mol, all other catalysts had imidazole bridge groups, which was the formation proof of ZIF-67 structure. Among the samples prepared by thermal dissolution method, the FTIR curve shape and peak position of CoFe7-ZIF and CoFe0-ZIF were most similar to that of CoFe0-ZIF as shown in **Figure 3A**. This indicated the formation of functional groups was consistent with the monometallic ZIF-67(Co) structure, when Fe doping amount was 7%mol. The absorption peaks around 1400 cm^{-1} and 1300 cm^{-1} changed obviously when the iron content was 14% and 21%. It was due to the substitution of cobalt by iron which caused the variations of C-N bond and Co-N bond.

When the content of iron reached to 100%mol, the FTIR curve changed significantly, due to the iron ion did not form an effective ZIF structure with the ligand of 2-methylimidazole, which was consistent with the test results of XRD.

In the samples of CoFe-ZIF-W prepared by the microwave dissolution method as shown in **Figure 3B**, it could be clearly seen that, in addition to the absorption peaks of the functional groups listed above, the characteristic peaks of Fe-O were also generated near 660 cm^{-1} and 560 cm^{-1} exhibited in the FTIR spectrums of CoFe7-ZIF-W, CoFe14-ZIF-W, CoFe21-ZIF-W and CoFe100-ZIF-W. Meanwhile, the Fe-O absorption peaks also appeared in CoFe21-ZIF and CoFe100-ZIF prepared by thermo dissolution method, further confirmed the iron oxides existence in the samples in accord with the characterization results of XRD. It was worth noting that 2-methylimidazole still produces a certain absorption peak in the sample prepared by the microwave dissolution method with Fe doping content of 21%, but the existence of ZIF structure was not detected in the XRD results. This was due to the small crystal size of its structure or the incomplete crystal grains.

In general, in the preparation of CoFe-ZIFs by thermo dissolution method, increasing the doping amount of iron changed the functional groups. When the Fe doping content was 7%, the effect on the functional group was small and it was not easy to detect in FTIR spectrum. When the Fe content was 14%mol or 21%mol, the FTIR curve changed significantly with the formation of iron oxides. In the CoFe-ZIF-W samples prepared by microwave dissolution methods, high-energy irradiation led to more energy blended into the bonds, changing the ZIF structure with more abundant and diverse functional groups. The mixed types of functional groups included both the intrinsic functional groups of ZIF and the new functional groups introduced by iron doping. Therefore, microwave dissolution methods were beneficial to construct more diverse functional group structures in ZIF, resulting in higher catalytic activity.

3.1.3 TG analysis

The TG analysis of synthesized catalysts were carried out under N_2 atmosphere in the range of 25–750°C, and the test results were shown in **Figure 4**. Before the heating process, all catalysts were activated at 150°C with the vacuum of 0.08 MPa. So, the weight loss exhibited in TG curve was mainly caused by the decomposition of the structure without physical adsorption water and chemical crystal water. In the samples prepared by thermo dissolution method as shown in **Figure 4A**, the structural decomposition temperature showed a decreasing trend with the Fe doping amount increasing. Among ZIF structure samples, CoFe21-ZIF had the lowest decomposition temperature and the deconstruction began at 374°C with weight losing about 30.2%. When the Fe doping amount was 14%, the decomposition temperature of the ZIF structure reached 478.7°C, which was about 14°C lower than that of the CoFe0-ZIF without Fe doping. It could be attributed to the substitution of iron for cobalt, which made more structural defects appear in ZIF structure. Although these structural defects improved the catalytic efficiency of catalyst, they also caused the reduction of the structural thermal stability. Except for CoFe100-ZIF, the other samples started to decompose above 350°C. It could be considered that the ZIF structure of the iron-cobalt bimetal bonds had good thermal stability. At the same time, we found there was a weight loss peak at around 280°C in CoFe100-ZIF which was caused by the

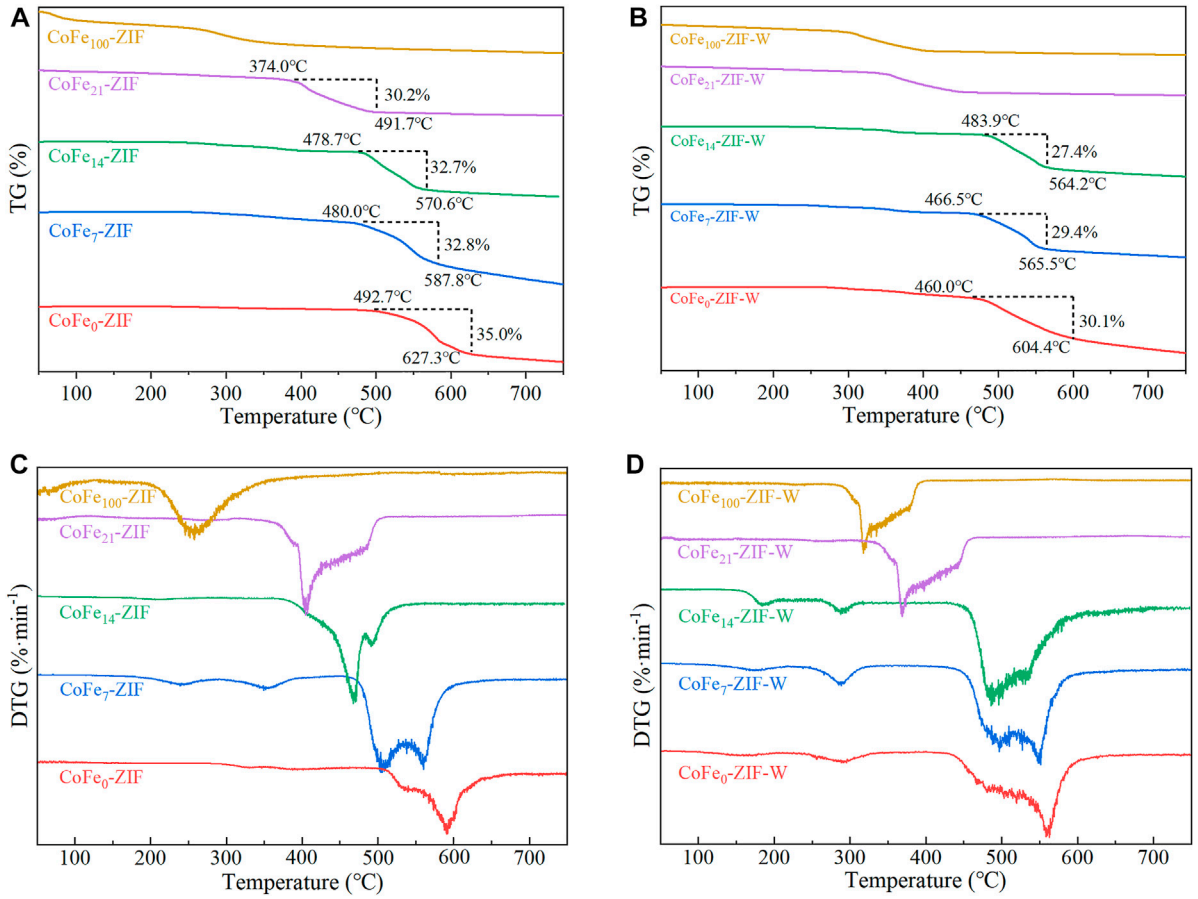

FIGURE 4 | TG analysis of catalysts under different preparation conditions **(A)** thermo dissolution method **(B)** microwave dissolution method **(C)** DTG of thermal dissolution method **(D)** DTG of microwave dissolution method.

volatilization of the residual ligand 2-methylimidazole, while the metal oxides crystals of Fe_2O_3 remained stable without significant weight loss.

Among the five materials prepared by microwave dissolution method as shown in **Figure 4B**, CoFe21-ZIF-W and CoFe100-ZIF-W had no obvious weight loss phenomenon, due to the relatively good thermal stability of main components of Fe_3O_4 and Fe_2O_3 crystals formed in the catalysts, which could be inferred from the XRD results. When the Fe doping amount was 0%mol, the decomposition temperature of CoFe0-ZIF-W was 460°C. When the Fe doping amount was 7%mol, the decomposition temperature of CoFe7-ZIF-W increased by 6.5–466.5°C. When the Fe doping content further rose to 14% mol, the decomposition temperature of CoFe14-ZIF-W also further improved, reaching 483.9°C, which was 23.9°C higher than that of CoFe0-ZIF-W, showing better thermal stability.

In addition, compared with the samples prepared by thermo dissolution method, the weight loss rate of the samples prepared by microwave dissolution method was relatively smaller. This indicated that the irradiation of microwaves not only promoted the formation of iron-containing oxides, but also improved the thermal stability of ZIF structure. At the same time, the result of CoFe21-ZIF-W sample exhibited the addition of excess Fe^{3+} did not improve the ZIF stability, and even destroyed the formation of ZIF structure resulting in iron oxides. In both CoFe100-ZIF and CoFe100-ZIF-W, the weight loss was significantly smaller than that of the other samples. It was because no valid ZIF structure was formed in the samples of CoFe100-ZIF and CoFe100-ZIF-W, and 2-methylimidazole did not form a ligand with the metal salt, but was washed away during the centrifugation. As a result, in the TG curve, there was no obvious weight loss caused by the massive decomposition of the ligand of 2-methylimidazole during the heating process.

3.1.4 SEM analysis

The morphology CoFe14-ZIF-W sample based on SEM test was shown in **Figure 5**. It could be obviously seen that the iron doping did not affect the typical morphology of ZIF-67 structure and only caused a small amount of distortion on each face of the ZIF dodecahedron. In **Figure 5B**, it can be seen more clearly that Fe_3O_4 crystal particles were attached to the surface of ZIF structure as a supported type. Based on the SEM image in **Figure 5B**, the particle size on the catalyst surface was about 20 nm.

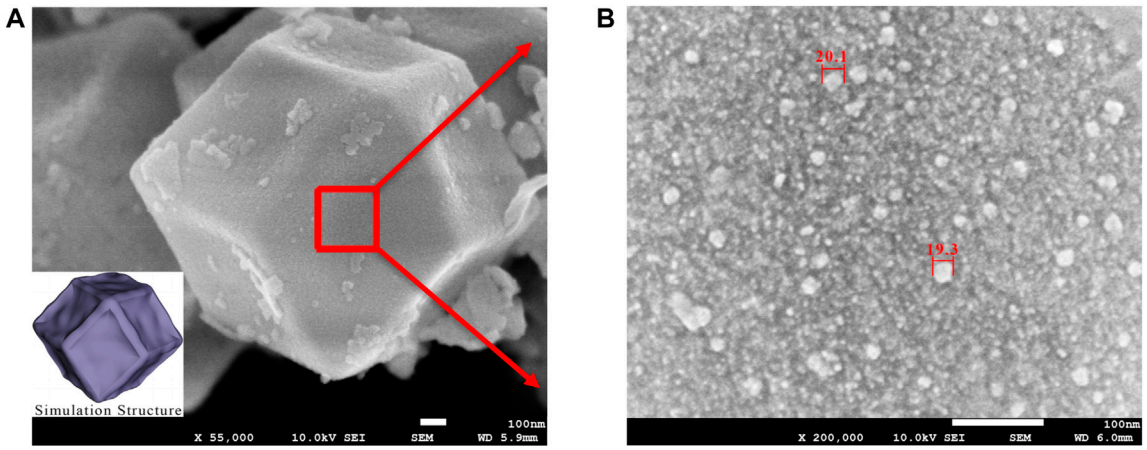

FIGURE 5 | SEM result of CoFe14-ZIF-W sample **(A)** SEM of a CoFe14-ZIF-W grain **(B)** Magnified SEM of the surface of the CoFe14-ZIF-W grain.

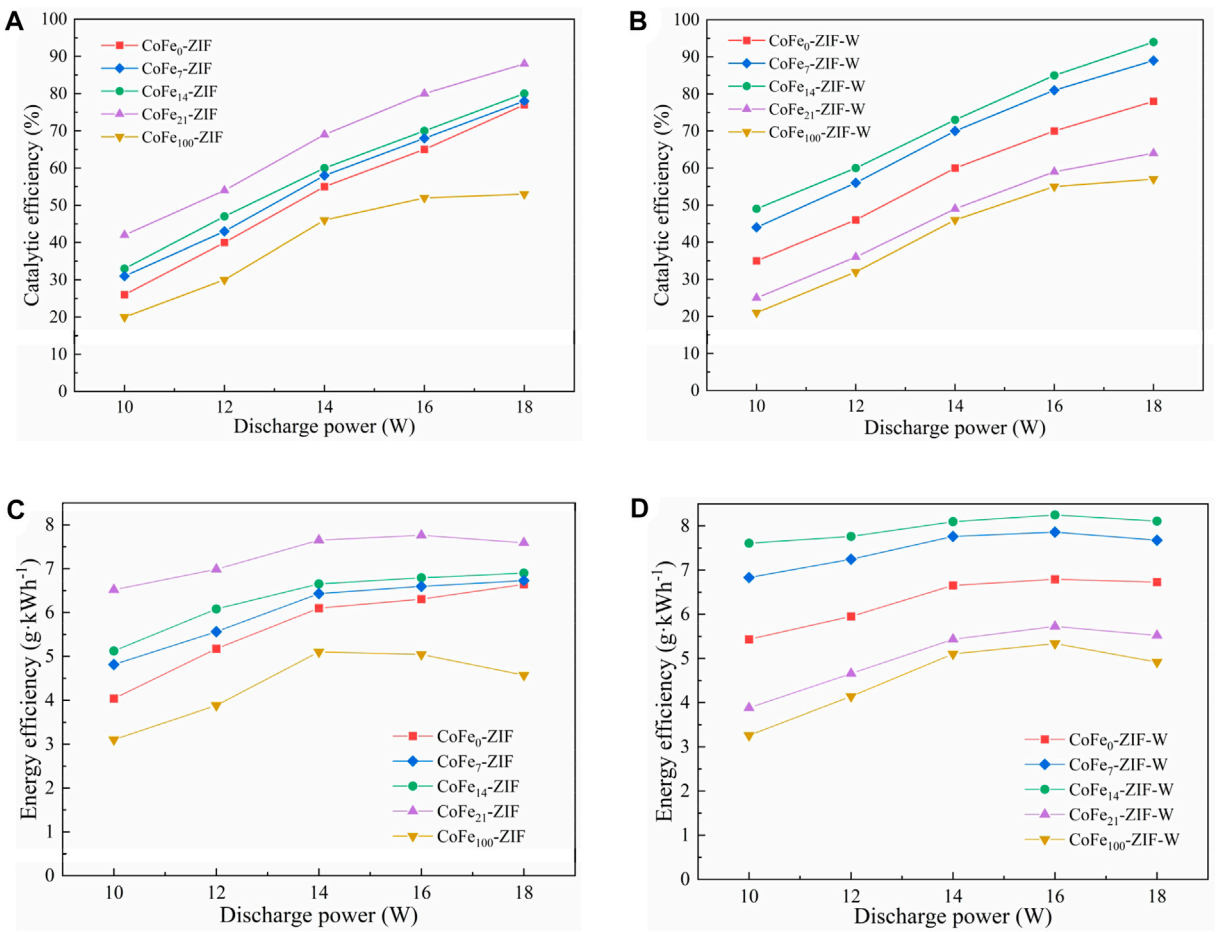

FIGURE 6 | Performance curves of different CoFe-ZIF(-W) samples for catalytic oxidation of α-pinene **(A)** catalytic efficiency of CoFe-ZIF samples **(B)** catalytic efficiency of CoFe-ZIF-W samples **(C)** energy efficiency of CoFe-ZIF samples **(D)** energy efficiency of CoFe-ZIF-W samples.

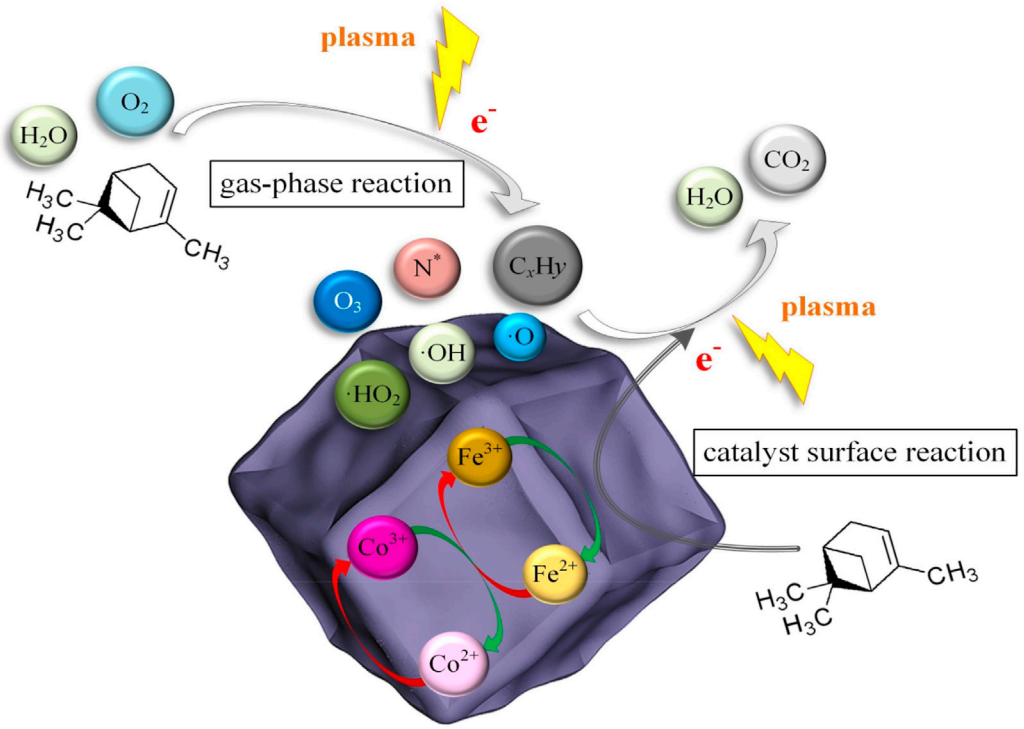

FIGURE 7 | Mechanism diagram of ZIF synergistic NTP catalyzing α-pinene oxidation.

3.2 Catalytic efficiency of CoFe-ZIFs for α-pinene

The efficiencies of CoFe-ZIFs synergistically with NTP to catalyze α-pinene oxidation under different discharge powers were shown in **Figure 6**.

Fe doping into ZIF structure could significantly improve the catalytic efficiency of the catalyst for α-pinene. Moreover, in all Fe-doped CoFe-ZIF(-W) samples, the catalytic efficiency increased with the rise of discharge power. This was because the increase of discharge power promoted the electric field strength in the plasma discharge region and the discharge generated more high-energy electrons and active species, thereby accelerating α-pinene oxidation. In addition, with the rise of discharge power, the energy efficiency showed a trend of first increasing and then decreasing. In the uptrend segment, the increase of the discharge power enhanced the number of high-energy electrons in the discharge region and greatly improved the probability of contact between α-pinene molecules and high-energy electrons, resulting in an enhance of the α-pinene catalytic efficiency. In the downtrend segment, part of input energy was used for the plasma discharge reaction, and the other part was dissipated in the form of heat. The higher the energy, the greater the proportion of heat loss, resulting in a decrease in energy efficiency.

In samples prepared by thermal dissolution method as shown in **Figures 6A,C**, when the discharge power increased from 10 to 18 W, the CoFe-ZIF with bimetal of iron and cobalt exhibited higher catalytic efficiency for α-pinene under the synergistic catalysis of NTP, in the order of CoFe21-ZIF > CoFe14-ZIF > CoFe7-ZIF > CoFe0-ZIF > CoFe100-ZIF. CoFe21-ZIF displayed the best catalytic effect of 92.6% at a discharge power of 18 W, which caused an increase of about 14.5% compared to the catalytic efficiency 78.1% of single-metal CoFe0-ZIF. At the same time, the energy efficiency was also improved from 6.52 g·kWh^{-1} of CoFe0-ZIF to 7.89 g·kWh^{-1} of CoFe21-ZIF. When the iron doping amount was 100%, the catalytic efficiency and energy efficiency of CoFe100-ZIF were greatly reduced.

Among the samples prepared by microwave dissolution method as shown in **Figures 6B,D**, the catalytic efficiency of CoFe-ZIF-W for α-pinene also increased with the discharge power rising and the energy efficiency also showed a trend of increasing first and then decreasing, quite similar to those of CoFe-ZIF samples. When the iron doping amount was 14%, its catalytic efficiency was the highest at various discharge powers, achieving 94.3% at 18W, and the energy efficiency obtained 8.11 g·kWh^{-1}. Moreover, the synergistic catalytic effect of CoFe21-ZIF-W or CoFe100-ZIF-W with NTP for α-pinene was similar without reaching a high level.

These results indicated that compared with the samples without ZIF structure, the CoFe-ZIF(-W) samples in the form of typical ZIF structure was more sensitive to α-pinene molecules and discharge-generated active species (such as O, ·OH and O_3) with stronger adsorption capacity. The active substances adsorbed on the surface of ZIF further reacted with α-pinene molecules and intermediate products, thereby prolonging the actual reaction time of the active particles in the reactor, changing the degree of aggregation, and increasing the probability of the reaction between the active substance and the α-pinene molecule, so as to more effectively catalyze α-

pinene. During the experiments, the generations of N_2O, NO and NO_2 were monitored, but there was no detectable concentration under any test condition. It could be due to the low discharge power of NTP, the strong catalytic activity and high catalytic selectivity of CoFe-ZIF(-W) samples.

3.3 Mechanism Analysis

The synergistic catalysis of α-pinene by CoFe-ZIF(-W) and NTP is a complex physicochemical process, including gas-phase reaction and catalyst surface reaction as shown in **Figure 7**. The gas phase reaction process mainly includes two ways (Lukes et al., 2012; Karatum and Deshusses, 2016). One is that the high-energy electrons generate by the discharge of the device directly collide and react with α-pinene molecules. When the electrons energy is higher than the chemical bonds energy, the α-pinene is broken to form a series of small molecule compounds. The other is that high-energy electrons collide with background gases (such as N_2, O_2, H_2O, etc.) to generate active particles (such as O, O_3, N*, ·OH, $\cdot HO_2$, etc.) with strong oxidizing ability (Guo et al., 2021a; Guo et al., 2021b). The active particles further react with α-pinene molecules or intermediates, resulting in deep oxidation destroying C-H, C=C or C-C bonds, and finally decompose and oxidize into H_2O and CO_2 (Liu et al., 2021).

The catalyst surface reaction is the oxidation reaction of adsorbed α-pinene or other intermediates with active particles on the surface of CoFe-ZIF(-W). The catalyst surface reaction is very important for the removal of α-pinene. The ZIF with outstanding adsorption ability can catch and enrich α-pinene, prolong the residence time of α-pinene in the reaction system, and increase the probability of intermolecular collision, thereby improving the catalytic efficiency. The oxidation reaction of α-pinene and its intermediates consume the surface active oxygen of CoFe-ZIF(-W), which require the continuous replenishment by lattice oxygen. In the active particles, O_3 adsorbed on the surface of CoFe-ZIF(-W) suffers a decomposition reaction to regenerate the lattice oxygen.

At present, the contribution of O_3 adsorption and decomposition on the surface of CoFe-ZIF(-W) to the synergistic catalysis has been recognized by many scholars (Tan et al., 2017; Yu et al., 2019; Peng et al., 2021). But the types of reactive oxygen species and the mechanism of action are yet to be determined, which requires in-depth research. In addition, the interaction between bimetallic iron and cobalt in CoFe-ZIF(-W) provides additional active centers that can enhance the generation and transfer of reactive oxygen species, thereby accelerating the deep oxidation of α-pinene and intermediates, producing CO_2 and H_2O.

4 CONCLUSION

In general, in the manufacturing process of briquette biofuel, the released terpenes such as pinene and camphene, as well as non-terpenoid VOCs such as formic acid, acetaldehyde, and benzene, have adverse effects on the clean utilization. We successfully synthesized composite catalysts of CoFe-ZIFs supporting Fe_3O_4 with high catalytic activity and high energy efficiency for α-pinene by microwave dissolution method. It was interesting that, under the co-irradiation of microwave, a small amount of Fe doping into CoFe-ZIF formed relatively stable Fe_3O_4 grains, and did not affect the bimetallic CoFe-ZIF forming. The introduction of microwave had a significant promoting effect on the formation of highly active Fe_3O_4 grains. The catalytic efficiency and energy efficiency of the composite catalyst CoFe-ZIF(-W) in α-pinene catalytic oxidation were higher than those of single-metal Co-ZIF catalyst or metal oxide catalyst (Fe_3O_4 or Fe_2O_3). Importantly, when Fe doping amount reached 21%, it inhibited CoFe-ZIF formation and reduced the performance of the catalyst. The microwave dissolution method could also be used to further synthesize MOFs structures of other elements and ligands, bimetallic carbides or bimetallic oxides, which is expected to be further applied in the fields of biofuel energy and environmental protection.

DATA AVAILABILITY STATEMENT

The original contributions presented in the study are included in the article/Supplementary Material, further inquiries can be directed to the corresponding author.

AUTHOR CONTRIBUTIONS

Conceptualization, YG, BC; Funding acquisition, YG; Methodology, SL, QW; Project administration, YG; Writing—original draft, YG, QC; Writing—review and editing, NG, GF, ZZ; Data curation, QC, HD.

FUNDING

Shandong Natural Science Foundation (ZR2019PEE002), China Postdoctoral Science Foundation (2020M671983), Postdoctoral Innovation Project of Shandong Province (202103077).

REFERENCES

Bermudez, J. H., Rojas, G., Benitez, R. B., and Franco, J. M. (2020). Easy Epoxidation of Monoterpenes from Common Starting Materials. *J. Braz. Chem. Soc.* 31 (5), 1086–1092. doi:10.21577/0103-5053.20190253

Bhatia, S. K., Jagtap, S. S., Bedekar, A. A., Bhatia, R. K., Patel, A. K., Pant, D., et al. (2020). Recent Developments in Pretreatment Technologies on Lignocellulosic Biomass: Effect of Key Parameters, Technological Improvements, and Challenges. *Bioresour. Technol.* 300, 122724. doi:10.1016/j.biortech.2019.122724

Chen, Q., Zhang, X., Li, S., Tan, J., Xu, C., Huang, Y., et al. (2020). MOF-Derived Co_3O_4@Co-Fe Oxide Double-Shelled Nanocages as Multi-Functional Specific Peroxidase-like Nanozyme Catalysts for Chemo/biosensing and Dye Degradation. *Chem. Eng. J.* 395, 125130. doi:10.1016/j.cej.2020.125130

Cheng, Z., Li, C., Chen, D., Chen, J., Zhang, S., Ye, J., et al. (2019). A Novel Array of Double Dielectric Barrier Discharge Combined with TiCo Catalyst to Remove High-Flow-Rate Toluene: Performance Evaluation and Mechanism Analysis. *Sci. Total Environ.* 692, 940–951. doi:10.1016/j.scitotenv.2019.07.318

Englund, F., and Nussbaum, R. M. (2000). Monoterpenes in Scots Pine and Norway Spruce and Their Emission during Kiln Drying. *Holzforschung* 54 (5), 449–456. doi:10.1515/HF.2000.075

Feng, X., Chen, C., He, C., Chai, S., Yu, Y., Cheng, J., et al. (2020). Non-thermal Plasma Coupled with MOF-74 Derived Mn-Co-Ni-O Porous Composite Oxide for Toluene Efficient Degradation. *J. Hazard. Mater.* 383, 121143. doi:10.1016/j.jhazmat.2019.121143

Foong, S. Y., Liew, R. K., Yang, Y., Cheng, Y. W., Yek, P. N. Y., Wan Mahari, W. A., et al. (2020). Valorization of Biomass Waste to Engineered Activated Biochar by Microwave Pyrolysis: Progress, Challenges, and Future Directions. *Chem. Eng. J.* 389, 124401. doi:10.1016/j.cej.2020.124401

Furukawa, H., Cordova, K. E., O'Keeffe, M., and Yaghi, O. M. (2013). The Chemistry and Applications of Metal-Organic Frameworks. *Science* 341 (6149), 1230444. doi:10.1126/science.1230444

Gao, Y., Jiang, W., Luan, T., Li, H., Zhang, W., Feng, W., et al. (2019a). High-Efficiency Catalytic Conversion of NOx by the Synergy of Nanocatalyst and Plasma: Effect of Mn-Based Bimetallic Active Species. *Catalysts* 9 (1), 103. doi:10.3390/catal9010103

Gao, Y., Luan, T., Peng, J., and Xu, H. (2013). Performance of V2O5-WO3-MoO_3/TiO_2 Catalyst for Diesel Engine NH3-SCR System. *CIESC J.* 64 (9), 3356–3366. doi:10.3969/j.issn.0438-1157.2013.09.038

Gao, Y., Luan, T., Zhang, M., Zhang, W., and Feng, W. (2018). Structure–Activity Relationship Study of Mn/Fe Ratio Effects on Mn–Fe–Ce–Ox/γ-Al_2O_3 Nanocatalyst for NO Oxidation and Fast SCR Reaction. *Catalysts* 8 (12), 642. doi:10.3390/catal8120642

Gao, Y., Luan, T., Zhang, S., Jiang, W., Feng, W., Jiang, H., et al. (2019c). Comprehensive Comparison between Nanocatalysts of Mn-Co/TiO2 and Mn-Fe/TiO_2 for NO Catalytic Conversion: An Insight from Nanostructure, Performance, Kinetics, and Thermodynamics. *Catalysts* 9 (2), 175. doi:10.3390/catal9020175

Gao, Y., Luan, T., Zhang, W., and Li, H. (2019b). The Promotional Effects of Cerium on the Catalytic Properties of Al_2O_3-Supported MnFeOx for NO Oxidation and Fast SCR Reaction. *Res. Chem. Intermed.* 45 (2), 663–686. doi:10.1007/s11164-018-3636-1

Gao, Y., Peng, X., Zhang, Z., Zhang, W., Li, H., Chen, B., et al. (2021a). Ternary Mixed-Oxide Synergy Effects of Nano TiO_2-FexOy-MOk (M = Mn, Ce, Co) on Alpha-Pinene Catalytic Oxidation Process Assisted by Nonthermal Plasma. *Mat. Res. Express* 8 (1), 015509. doi:10.1088/2053-1591/abdbf7

George, A., Shen, B., Craven, M., Wang, Y., Kang, D., Wu, C., et al. (2021). A Review of Non-Thermal Plasma Technology: A Novel Solution for CO_2 Conversion and Utilization. *Renew. Sustain. Energy Rev.* 135, 109702. doi:10.1016/j.rser.2020.109702

Guo, H., Li, Z., Lin, S., Li, D., Jiang, N., Wang, H., et al. (2021a). Multi-catalysis Induced by Pulsed Discharge Plasma Coupled with Graphene-Fe_3O_4 Nanocomposites for Efficient Removal of Ofloxacin in Water: Mechanism, Degradation Pathway and Potential Toxicity. *Chemosphere* 265, 129089. doi:10.1016/j.chemosphere.2020.129089

Guo, H., Li, Z., Xiang, L., Jiang, N., Zhang, Y., Wang, H., et al. (2021b). Efficient Removal of Antibiotic Thiamphenicol by Pulsed Discharge Plasma Coupled with Complex Catalysis Using Graphene-WO3-Fe_3O_4 Nanocomposites. *J. Hazard. Mater.* 403, 123673. doi:10.1016/j.jhazmat.2020.123673

Guo, H., Wang, Y., Yao, X., Zhang, Y., Li, Z., Pan, S., et al. (2021c). A Comprehensive Insight into Plasma-Catalytic Removal of Antibiotic Oxytetracycline Based on Graphene-TiO_2-Fe_3O_4 Nanocomposites. *Chem. Eng. J.* 425, 130614. doi:10.1016/j.cej.2021.130614

Guo, Y., Wen, M., Li, G., and An, T. (2021d). Recent Advances in VOC Elimination by Catalytic Oxidation Technology onto Various Nanoparticles Catalysts: a Critical Review. *Appl. Catal. B Environ.* 281, 119447. doi:10.1016/j.apcatb.2020.119447

Hu, Y., Kazemian, H., Rohani, S., Huang, Y., and Song, Y. (2011). *In Situ* high Pressure Study of ZIF-8 by FTIR Spectroscopy. *Chem. Commun.* 47 (47), 12694. doi:10.1039/C1CC15525C

Huang, H., Chen, C., Yang, R., Yu, Y., Albilali, R., He, C., et al. (2020). Remarkable Promotion Effect of Lauric Acid on Mn-MIL-100 for Non-thermal Plasma-Catalytic Decomposition of Toluene. *Appl. Surf. Sci.* 503, 144290. doi:10.1016/j.apsusc.2019.144290

Ikreedeegh, R. R., and Tahir, M. (2021). A Critical Review in Recent Developments of Metal-Organic-Frameworks (MOFs) with Band Engineering Alteration for Photocatalytic CO_2 Reduction to Solar Fuels. *J. CO2 Util.* 43, 101381. doi:10.1016/j.jcou.2020.101381

Jamshidifard, S., Koushkbaghi, S., Hosseini, S., Rezaei, S., Karamipour, A., Jafari rad, A., et al. (2019). Incorporation of UiO-66-NH2 MOF into the PAN/chitosan Nanofibers for Adsorption and Membrane Filtration of Pb(II), Cd(II) and Cr(VI) Ions from Aqueous Solutions. *J. Hazard. Mater.* 368, 10–20. doi:10.1016/j.jhazmat.2019.01.024

Karatum, O., and Deshusses, M. A. (2016). A Comparative Study of Dilute VOCs Treatment in a Non-thermal Plasma Reactor. *Chem. Eng. J.* 294, 308–315. doi:10.1016/j.cej.2016.03.002

Lee, J.-G., Chae, Y., Shin, Y., and Kim, Y.-J. (2020). Chemical Composition and Antioxidant Capacity of Black Pepper Pericarp. *Appl. Biol. Chem.* 63 (1), 35. doi:10.1186/s13765-020-00521-1

Li, H.-Y., Zhao, S.-N., Zang, S.-Q., and Li, J. (2020a). Functional Metal–Organic Frameworks as Effective Sensors of Gases and Volatile Compounds. *Chem. Soc. Rev.* 49 (17), 6364–6401. doi:10.1039/C9CS00778D

Li, N., Zhou, L., Jin, X., Owens, G., and Chen, Z. (2019). Simultaneous Removal of Tetracycline and Oxytetracycline Antibiotics from Wastewater Using a ZIF-8 Metal Organic-Framework. *J. Hazard. Mater.* 366, 563–572. doi:10.1016/j.jhazmat.2018.12.047

Li, T., Chen, C., Brozena, A. H., Zhu, J. Y., Xu, L., Driemeier, C., et al. (2021). Developing Fibrillated Cellulose as a Sustainable Technological Material. *Nature* 590 (7844), 47–56. doi:10.1038/s41586-020-03167-7

Li, X., Zhang, L., Yang, Z., Wang, P., Yan, Y., Ran, J., et al. (2020b). Adsorption Materials for Volatile Organic Compounds (VOCs) and the Key Factors for VOCs Adsorption Process: A Review. *Sep. Purif. Technol.* 235, 116213. doi:10.1016/j.seppur.2019.116213

Li, Z. S., Luo, G. Y., Chen, T., Zeng, Z., Guo, S. X., Lv, J., et al. (2020c). Bimetallic CoCu Catalyst Derived from *In-Situ* Grown Cu-ZIF-67 Encapsulated inside KIT-6 for Higher Alcohol Synthesis from Syngas. *FUEL* 278, 118292. doi:10.1016/j.fuel.2020.118292

Liu, R., Song, H., Li, B., Li, X., and Zhu, T. (2021). Simultaneous Removal of Toluene and Styrene by Non-thermal Plasma-Catalysis: Effect of VOCs Interaction and System Configuration. *Chemosphere* 263, 127893. doi:10.1016/j.chemosphere.2020.127893

Lu, W., Abbas, Y., Mustafa, M. F., Pan, C., and Wang, H. (2019). A Review on Application of Dielectric Barrier Discharge Plasma Technology on the Abatement of Volatile Organic Compounds. *Front. Environ. Sci. Eng.* 13 (2), 30. doi:10.1007/s11783-019-1108-5

Lukes, P., Locke, B. R., and Brisset, J. L. (2012). Aqueous-phase Chemistry of Electrical Discharge Plasma in Water and in Gas–Liquid Environments. *Plasma Chem. Catal. Gases Liq.*, 243–308. doi:10.1002/9783527649525.ch7

Machado, C. D., Raman, V., Rehman, J. U., Maia, B. H. L. N. S., Meneghetti, E. K., Almeida, V. P., et al. (2019). Schinus Molle: Anatomy of Leaves and Stems, Chemical Composition and Insecticidal Activities of Volatile Oil against Bed Bug (Cimex Lectularius). *Rev. Bras. Farmacogn.* 29 (1), 1–10. doi:10.1016/j.bjp.2018.10.005

Manisalidis, I., Stavropoulou, E., Stavropoulos, A., and Bezirtzoglou, E. (2020). Environmental and Health Impacts of Air Pollution: A Review. *Front. Public Health* 8, 14. doi:10.3389/fpubh.2020.00014

Pekgozlu, A. K., and Ceylan, E. (2018). Chemical Compostion of Taurus Fir (Abies Cilicica Subsp Isaurica) Oleoresin. *Rev. Arvore* 42 (1), 100015. doi:10.1590/1806-90882018000100015

Peng, J., He, Y., Zhou, C., Su, S., and Lai, B. (2021). The Carbon Nanotubes-Based Materials and Their Applications for Organic Pollutant Removal: A Critical Review. *Chin. Chem. Lett.* 32 (5), 1626–1636. doi:10.1016/j.cclet.2020.10.026

Qiu, M., Liu, Z., Wang, S., and Hu, B. (2021). The Photocatalytic Reduction of U(VI) into U(IV) by ZIF-8/g-C3n4 Composites at Visible Light. *Environ. Res.* 196, 110349. doi:10.1016/j.envres.2020.110349

Safaei, M., Foroughi, M. M., Ebrahimpoor, N., Jahani, S., Omidi, A., Khatami, M., et al. (2019). A Review on Metal-Organic Frameworks: Synthesis and Applications. *TrAC Trends Anal. Chem.* 118, 401–425. doi:10.1016/j.trac.2019.06.007

Shi, J., Qiu, F., Yuan, W., Guo, M., and Lu, Z.-H. (2021). Nitrogen-doped Carbon-Decorated Yolk-Shell CoP@FeCoP Micro-polyhedra Derived from MOF for Efficient Overall Water Splitting. *Chem. Eng. J.* 403, 126312. doi:10.1016/j.cej.2020.126312

Tan, X., Wan, Y., Huang, Y., He, C., Zhang, Z., He, Z., et al. (2017). Three-dimensional MnO_2 Porous Hollow Microspheres for Enhanced Activity as Ozonation Catalysts in Degradation of Bisphenol A. *J. Hazard. Mater.* 321, 162–172. doi:10.1016/j.jhazmat.2016.09.013

Vakili, R., Gholami, R., Stere, C. E., Chansai, S., Chen, H., Holmes, S. M., et al. (2020). Plasma-assisted Catalytic Dry Reforming of Methane (DRM) over Metal-Organic Frameworks (MOFs)-Based Catalysts. *Appl. Catal. B Environ.* 260, 118195. doi:10.1016/j.apcatb.2019.118195

Vandenbroucke, A. M., Morent, R., De Geyter, N., and Leys, C. (2011). Non-thermal Plasmas for Non-catalytic and Catalytic VOC Abatement. *J. Hazard. Mater.* 195, 30–54. doi:10.1016/j.jhazmat.2011.08.060

Wang, X., Yu, L., Guan, B. Y., Song, S., and Lou, X. W. (2018). Metal–Organic Framework Hybrid-Assisted Formation of Co_3O_4/Co-Fe Oxide Double-Shelled Nanoboxes for Enhanced Oxygen Evolution. *Adv. Mat.* 30 (29), 1801211. doi:10.1002/adma.201801211

Wu, Z., Wang, Y., Xiong, Z., Ao, Z., Pu, S., Yao, G., et al. (2020). Core-shell Magnetic Fe_3O_4@Zn/Co-ZIFs to Activate Peroxymonosulfate for Highly Efficient Degradation of Carbamazepine. *Appl. Catal. B Environ.* 277, 119136. doi:10.1016/j.apcatb.2020.119136

Yaghi, O. M., Li, G., and Li, H. (1995). Selective Binding and Removal of Guests in a Microporous Metal–Organic Framework. *Nature* 378 (6558), 703–706. doi:10.1038/378703a0

Yoo, C. G., Meng, X., Pu, Y., and Ragauskas, A. J. (2020). The Critical Role of Lignin in Lignocellulosic Biomass Conversion and Recent Pretreatment Strategies: A Comprehensive Review. *Bioresour. Technol.* 301, 122784. doi:10.1016/j.biortech.2020.122784

Yu, D., Wu, M., Hu, Q., Wang, L., Lv, C., Zhang, L., et al. (2019). Iron-based Metal-Organic Frameworks as Novel Platforms for Catalytic Ozonation of Organic Pollutant: Efficiency and Mechanism. *J. Hazard. Mater.* 367, 456–464. doi:10.1016/j.jhazmat.2018.12.108

Zhang, E., Xie, Y., Ci, S., Jia, J., and Wen, Z. (2016). Porous Co_3O_4 Hollow Nanododecahedra for Nonenzymatic Glucose Biosensor and Biofuel Cell. *Biosens. Bioelectron.* 81, 46–53. doi:10.1016/j.bios.2016.02.027

Zhang, T., Zhang, X., Yan, X., Kong, L., Zhang, G., Liu, H., et al. (2013). Synthesis of Fe3O4@ZIF-8 Magnetic Core–Shell Microspheres and Their Potential Application in a Capillary Microreactor. *Chem. Eng. J.* 228, 398–404. doi:10.1016/j.cej.2013.05.020

Zhang, X., Ji, G., Liu, W., Quan, B., Liang, X., Shang, C., et al. (2015). Thermal Conversion of an Fe_3O_4@metal–Organic Framework: a New Method for an Efficient Fe–Co/nanoporous Carbon Microwave Absorbing Material. *Nanoscale* 7 (30), 12932–12942. doi:10.1039/C5NR03176A

Zhang, X., Yang, Y., Song, L., Wang, Y., He, C., Wang, Z., et al. (2018). High and Stable Catalytic Activity of Ag/Fe2O3 Catalysts Derived from MOFs for CO Oxidation. *Mol. Catal.* 447, 80–89. doi:10.1016/j.mcat.2018.01.007

Zheng, F., He, M., Yang, Y., and Chen, Q. (2015). Nano Electrochemical Reactors of Fe_2O_3 Nanoparticles Embedded in Shells of Nitrogen-Doped Hollow Carbon Spheres as High-Performance Anodes for Lithium-Ion Batteries. *Nanoscale* 7 (8), 3410–3417. doi:10.1039/C4NR06321J

Zhou, K., Mousavi, B., Luo, Z., Phatanasri, S., Chaemchuen, S., Verpoort, F., et al. (2017). Characterization and Properties of Zn/Co Zeolitic Imidazolate Frameworks vs. ZIF-8 and ZIF-67. *J. Mat. Chem. A Mat.* 5 (3), 952–957. doi:10.1039/C6TA07860E

Zhou, R., Zhou, R., Alam, D., Zhang, T., Li, W., Xia, Y., et al. (2021). Plasmacatalytic Bubbles Using CeO_2 for Organic Pollutant Degradation. *Chem. Eng. J.* 403, 126413. doi:10.1016/j.cej.2020.126413

Zhu, L., Shen, D., and Luo, K. H. (2020). A Critical Review on VOCs Adsorption by Different Porous Materials: Species, Mechanisms and Modification Methods. *J. Hazard. Mater.* 389, 122102. doi:10.1016/j.jhazmat.2020.122102

Zou, W. H., Guo, Y. X., Li, P., Liu, M. Y., and Hou, L. X. (2021). Bimetallic-organic Frameworks CoMo-ZIF-67: An Efficient and Stable Catalyst for Selective Oxidation of Alkenes. *CHEMCATCHEM* 13 (1), 416–424. doi:10.1002/cctc.202001368

Conflict of Interest: The authors declare that the research was conducted in the absence of any commercial or financial relationships that could be construed as a potential conflict of interest.

The handling editor JS declared a shared parent affiliation with the author(s) at the time of review.

Publisher's Note: All claims expressed in this article are solely those of the authors and do not necessarily represent those of their affiliated organizations, or those of the publisher, the editors and the reviewers. Any product that may be evaluated in this article, or claim that may be made by its manufacturer, is not guaranteed or endorsed by the publisher.